Electronic Supplementary Material (ESI) for Lab on a Chip.

Electronic Supplementary Information for

Portable Light-sheet Optofluidic Microscopy for 3D Fluorescence Imaging Flow Cytometry

Jeonghwan Son,[a] Biagio Mandracchia,[a] Aaron D. Silva Trenkle,[a] Gabriel A. Kwong[ab] and Shu Jia[ab*]

[a] Wallace H. Coulter Department of Biomedical Engineering, Georgia Institute of Technology and Emory University, Atlanta, GA, USA
[b] Parker H. Petit Institute of Bioengineering and Bioscience, Georgia Institute of Technology, Atlanta, GA 30332, USA
* Corresponding author: shu.jia@gatech.edu

Supplementary Note 1. Sample preparation.

1. Fluorescent beads preparation.

The fluorescent beads slide was prepared to measure systemic point-spread-function shown in **Fig. 2**. We used 5 µL of the 200 nm diameter of fluorescent beads (T7280, TetraSpeck beads, Invitrogen) directly on a sample slide (48312-003, VWR) with a glass cover (48306-227, 170 µm thickness, VWR). For the floating mixture of beads shown in **Fig. 3**, we mixed 1 mL of the 7 µm diameter (FSFR007, Uniform Dyed Microspheres) and 15 µm diameter (F7238, FocalCheck Microspheres, Invitrogen) in a diluted water solution.

2. HeLa and Jurkat cell preparation.

HeLa and Jurkat cells were directly purchased from Millipore Sigma and maintained healthy status inside an incubator. HeLa cells were cultured in complete DMEM (Corning, 12721007). Jurkat cells were cultured in complete RPMI (2mM L-Glut and 10% FBS, Glibco). Both cells were washed twice with HBSS (Corning, 09822004) before any staining protocols.

3. Isolated Human T cell preparation.

Human peripheral blood mononuclear cells (PBMCs) were collected from healthy human donors approved as IRB #H 20288 by Georgia Tech and Emory University Institutional Review Boards and isolated by Lymphoprep density gradient medium (STEMCELL Technologies, #07801) in SepMate-15mL tubes (STEMCELL Technologies, #85415). Next, human T cells (CD3+) were isolated by EasySep Human CD3 Positive Selection Kit II (STEMCELL Technologies, 17851) and activated using Dynabeads (ThermoFisher, #11131D) with the ratio of 3:1 (bead-to-cell). The prepared mixtures of activated cells were cultured in complete human T cell media (hTCM; X-vivo 10, Lonza #04-380Q), 5% Human AB serum (Valley Biomedical, #HP1022), 10 mM N-acetyl L-Cysteine (Sigma Aldrich, #A9165), and 55 µM 2-mercaptoethanol (Sigma Aldrich, #M3148-100mL). The cultured cells were supplemented with 50 µ/mL recombinant human IL-2 (TECIN™ Teceleukin, Bulk Ro 23-6019, National Cancer Institute, Frederick, MD) every other day to maintain cells at a concentration of 7×10^5 to 2×10^6 cells/mL. On Day 7 of culture, T cells were supplemented again with Dynabeads at the ratio of 1:1 (bead-to-cell). On Day 9, the added beads were removed from the media, and human T cells were maintained at a concentration of 7×10^5 to 2×10^6 cells/mL.

4. Cell staining.

The plasma membranes of cells were stained according to the protocol (Cell Mask Deep Red Plasma Membrane Stain, #C10046, Invitrogen) for 30 minutes inside an incubator maintained at 37°C and 5% CO_2 level. The nuclei of the cells were stained with SYTOX Deep Red Nucleic Acid Stain (Invitrogen, #S11381), which penetrates cells with the compromised plasma membrane of fixed and dead cells. After the staining process and washing with HBSS to limit the potential overloads of staining solutions, we split the cells with Trypsin and permeabilized them by adding 4% Paraformaldehyde fixative solutions for 10 minutes. After centrifuging samples for 5 minutes with 0.02 g/minutes speed (AccuSpin Micro17, Fisher Scientific), we washed samples twice and stored them with 0.5M EDTA (UltraPure 0.5M EDTA, pH 8.0, #2187281, Invitrogen) for the experiments. The EDTA buffer also prevents cell-to-cell adhesion and clumping[1].

5. Cytotoxicity assay.

For the cytotoxicity test in **Fig. 5**, 1 mM of Paclitaxel (Taxol, #P3456, Invitrogen) stock was prepared according to the protocol provided by the distributor (Invitrogen). We administered 400 nM of Taxol stock on live HeLa cells for 8 hours inside an incubator. The Taxol destabilizes the formation of cytoskeletons and induces apoptosis by blocking cell cycles [2, 3]. After the end of the application, we stained both the plasma membrane and nucleus and then fixed them according to the above cell staining protocol.

Supplementary Note 2. Image processing and 3D reconstruction.

We developed two approaches to reconstruct 3D-projected information from the image stack (x-y views) acquired by mechanical and flow scanning of the sample. The raw image stack was cropped to contain information from a single sample. Before the reconstruction process, all raw image stacks were processed with the open-source algorithm for the automatic correction of sCMOS-related noise (ACsN) to enhance signal-to-noise ratio[4].

The first approach is to measure the point-spread-function (PSF) of the system shown in **Fig. 2 (h-j)** and **Fig. S3 (a)**. To measure PSF with proper scale, the distance between neighboring frames should have identical gaps. The raw image stack of fluorescence beads on a glass slide was acquired by a mechanically controlled stage with a 1 μm step size in the scanning direction (S). After the ACsN processing, the image stack was then analyzed by an open-source algorithm[5] to accurately track the coordinates of the movement of PSF, **Fig. S3 (a, Tracking)**. Next, the coordinates of centroids of PSF were used to calibrate the location and frames to match with the mathematical locations that each 1 μm step size in scanning dimension should make about 3.5 pixels (1 [μm/step size] × cos (36°) / 240 [nm/pixel] = 3.37 [pixel/step]) movements in each image as **Fig. 1 (b, left)**. The mismatched location is mainly due to the lack of accuracy of the mechanical translation and sub-pixelation. A new image stack was generated by interpolating intensities to locate PSF in the calculated location, **Fig. S3 (a, Interpolating frames based on centroid locations)**. The interpolated frames had new coordinates of centroids of PSF with identical pixel gaps (i.e., about 3.5-pixel differences between frames). Next, we sheared the reconstructed image stacks by the pixel movement (about 3.5 pixels) to realign the image stack from the scanning direction (S) to the optical axis direction (Z) as **Fig. S3 (a. Realignment)**. The reconstructed voxel has a dimension of 240 nm × 240 nm × 587 nm (= 1 μm × sin(36°)) at no image binning.

The second approach is to reconstruct 3D information of the sample acquired by flow scanning shown in **Fig. 3-5** and **Fig. S3 (b)**. The variances of the flow speed may generate non-consistent scanning gaps between neighboring frames, which ultimately results in scaling issues. Hence, we customized the reconstruction approach to interpolate information. First, the image stack of samples was acquired with flow scanning at a static flow rate, **Fig. S3 (b, Raw image stack from flow scanning)**. Next, the image stack was analyzed to generate a perspective view (kymography) in the X-Z dimension, **Fig. S3 (b, Kymograph)**. By estimating the centroids of the mass of intensities of the sample in each frame, the missing frames were identified. Here, we set the differences of centroid as 1 pixel (480 nm at 2x2 image binning) for simplification. Next, the intensities of the sample were interpolated to generate a new image stack. As a result, the final image stack had the identical distance of centroids (1 pixel) of the sample between neighboring frames. The centroid coordinates were fitted with a spline function, **Fig. S3 (b, Interpolating frames & finding centroids)**. With the fitted slope of the centroids of the z-dependent kymograph, the image stack was linearly translated to realign the image stack from flow direction (S) to optical axis direction (Z), **Fig. S3 (b, Shearing)**. The reconstructed voxel has a dimension of 480 nm × 480 nm × 282 nm (= 480 nm × sin(36°)) at 2x2 binning. After the reconstruction, the deconvolution (50 iterations with the Richardson-Lucy approach, DeconvolutionLab2[6], Fiji) was performed to enhance the resolution and image quality.

Supplementary Note 3. Volume and NV/PV ratio estimation.

The process to estimate volume uses the edge-based area detection frame-by-frame in the image stack, **Fig. S4 (a)**. First, a deconvoluted image stack was processed to segment the effective pixels via thresholding with the Sobel operator and edge detection, **Fig. S4 (a, Thresholding & Edge detection)**. The binary mask was then generated by eliminating separate border lines via dilating with linear structuring elements and filling the internal pixels, **Fig. S4 (a, Binary mask & Cleaning borders)**. The overall approach was modified from the open-sourced approach (Detect Cell Using Edge Detection and Morphology process, MATLAB) and the reference[7]. With the processed image stack of binary masks, we calculated the estimated volume of the sample by multiplying the total number of effective pixels in the image stack with a single voxel size (480 nm × 480 nm × 480 nm) at 2×2 image binning.

The process to differentiate the viability of the cells in the cytotoxicity test uses the size of the plasma membrane-stained structure, the volume stack from the volume estimation process, and two fluorescence staining reagents. First, we stained the plasma membrane and nucleus of HeLa cells after the administration of Paclitaxel (Taxol) for 8 hours inside an incubator. Unlike the plasma membrane staining that is permeable, SYTOX is a permeable dye only when the plasma membrane of cells becomes disrupted by chemotherapeutic agents. As results in **Fig. 4**, nuclei of drug-affected cells that possess compromised plasma membrane was labeled. Next, by analyzing the control groups, we decided the average size of the plasma membrane-stained structure (thickness) as about 15% of the largest radius of the 3D centroids calculated by Regionprops3 function (MATLAB), **Fig. S4 (b, left)**. We then segmented the cellular features and determined the volumetric ratio between fluorescence emitted from the nucleus (NV) and the plasma membrane (PV). NV was calculated by (1) the volumetric ellipticity calculated by Regionprops3 function (MATLAB) and (2) the distance from the 3D centroid to the plasma membrane. The effective nucleus volume was decided by double thresholds to refrain from including artifacts. As a result, the nucleus volume in 3D was estimated in **Fig. S4 (b, middle)**. Next, the NV/PV ratio was calculated by the total intensities of the effective nucleus volume and plasma membrane volume, **Fig. S4 (b, right)**. **Fig. S4 (c, d)** shows the estimated volume of the estimated nucleus and plasma membrane and color-coded projected images in 3D space. The overall two processes provide the estimation of volume measurement and NV/PV ratio to derive the efficacy of the cytotoxicity test.

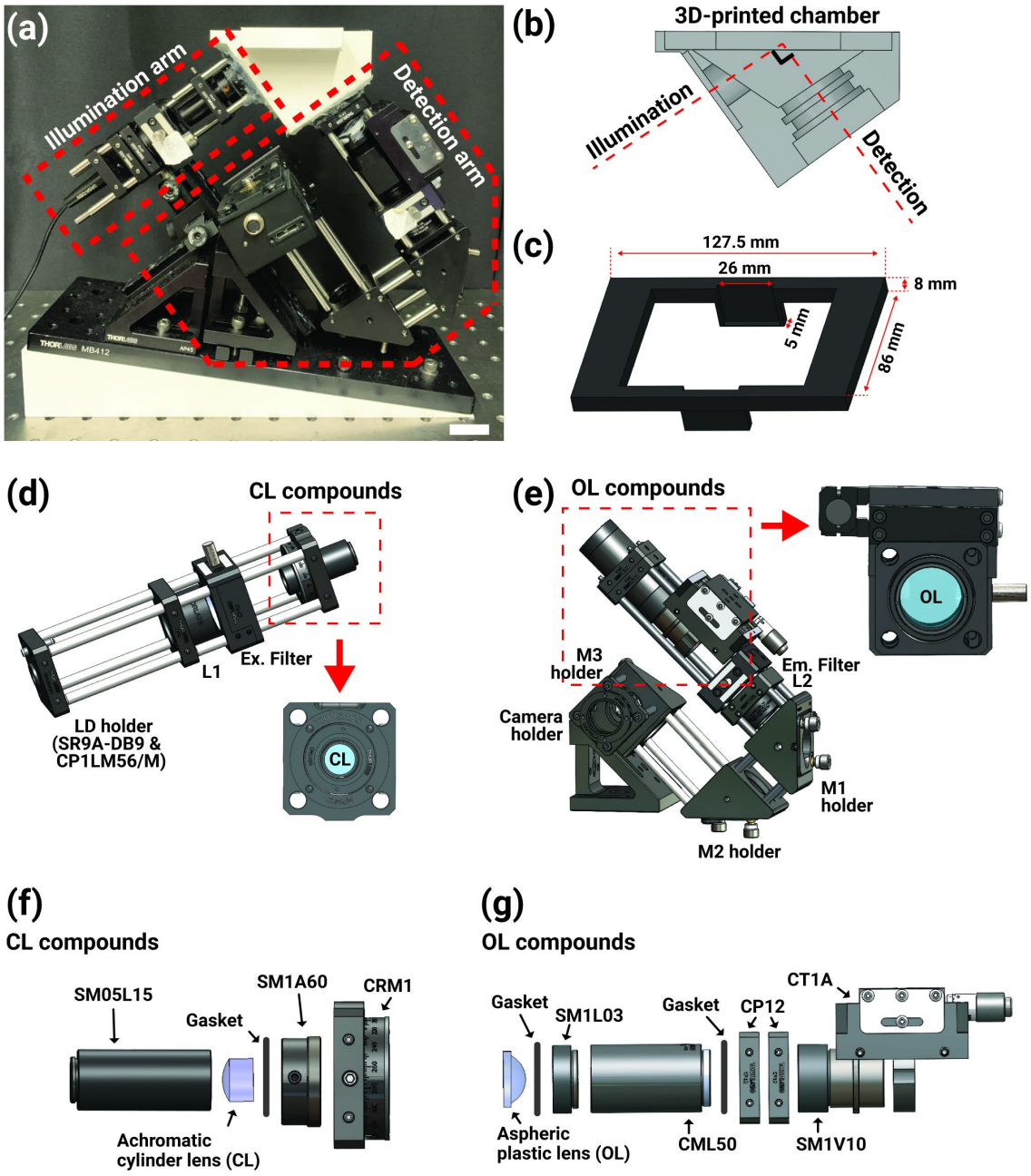

Supplementary Figure S1: Details of the PLSOM setup. (a) Photograph of the system and the optical paths. The system has consisted of a 3D-printed chamber, an illumination arm, and a detection arm. (b) The cross-sectional image of a 3D-printed chamber rendered by computer-aid software (SolidWorks). The chamber was designed to contain the immersion water and secure the positions of the CL, OL, and microfluidic chips. (c) A microfluidic chip is secured on a customized sample holder and support (#I3020, ASIimaging) and located to focal planes by a 1-axis translation stage. (d) The illumination arm has consisted of cylinder lens (CL) compounds, an excitation filter, a collimating lens (L3), and a laser diode (LD) holder. As a red color dotted box in (d), CL is secured by a rubber gasket preventing potential leakage of immersion water. (e) The side view of the detection arm. It has objective lens (OL) compounds, an emission filter, a tube lens (L4), three reflective mirrors (M1-3), and a camera holder. As a red color dotted box in (d), OL is secured with a rubber gasket. The folded optical pathways enable the reduction in the overall length of the detection pathway (about 30 cm), thus providing portability of PLSOM. The distance was calculated to meet the Nyquist requirement. The rendering images of CL compounds (f) and OL compounds (g). Each compound has an optical lens, rubber gasket, and supports. Scale bar: 25 mm (a).

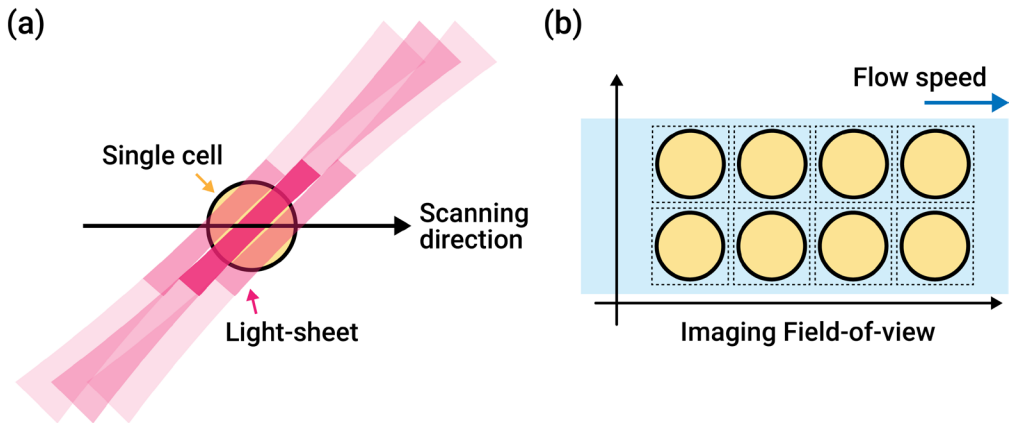

Supplementary Figure S2: The flow speed and corresponding analytic throughput of the PLSOM system. (a) Illustration of the geographical relationship of a single cell and light sheet. With the single cell with an average diameter of 10 µm and the thickness of the light sheet (~4 µm) in the PLSOM system, at least three consecutive frames are required to cover the entire size of the single cell. The camera exposure time used in the experiment (16 ms) results in the maximum speed limit of the flow below 206 µm/sec. (b) Illustration of the analytic throughput calculation. Dotted squares with single cells illustrate the confined area to calculate the throughput. The maximum analytic throughput of the system can be derived by factoring the highest density of the cell (100%) of cells with an average cell volume (1,000 μm^3) moving with the flow speed limit (206 µm/sec) within the imaging field-of-view (~15 µm x 490 µm). Here, our analytic throughput (~1,180 cells/sec = 15 µm × 492 µm × 80 % × 200 µm / 1,000 μm^3) was calculated at 80% of cell density in the channel.

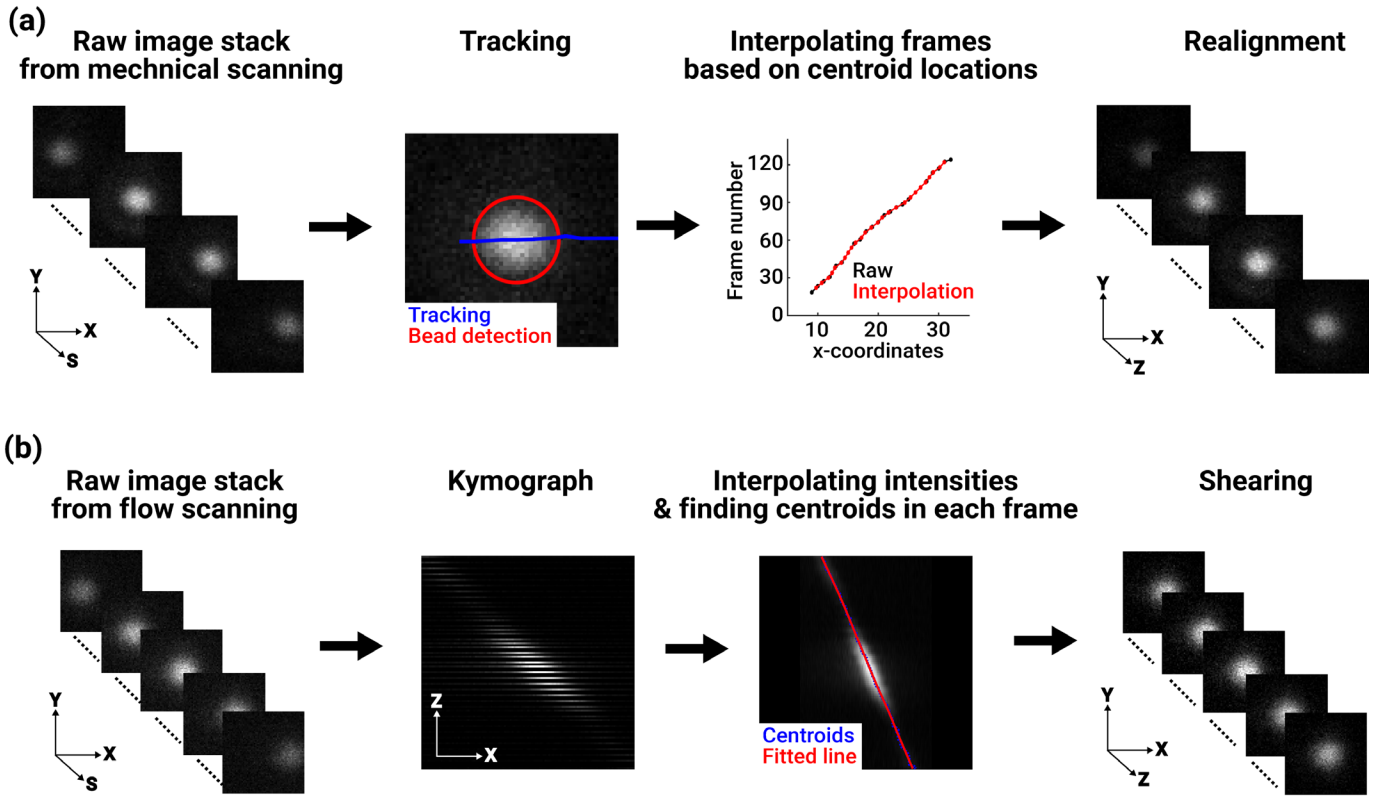

Supplementary Figure S3: Volumetric reconstruction process. (a) The process to reconstruct the point-spread-function (PSF) acquired from mechanically scanning. The sample stage was controlled to move the sample slide with a 1 μm step size in the scanning direction (s). The light-sheet illumination at an angle of 36 ° with respect to the horizontal sample plane results in about 3.5 pixels of transition of the centroids of PSF in each image. The open-sourced tracking enables the accurate estimate of the centroids, supporting to interpolate frames. New image stack was generated by interpolating intensities based on interpolated centroid location (x-coordinate). Next, the final image stack was realigned by shearing with about 3.5 pixels to relocate the image stack from the scanning direction to the optical axis direction (z). (b) The process to reconstruct 3D information of the image stack acquired from flow scanning. After the raw image stack was acquired at the controlled flow speed, the kymograph in the x-z dimension was generated. The missing frames were identified according to the centroid of the intensity of the sample in each image stack. The variance of flow speed inside a microfluidic channel may generate a lack of information captured by a camera acquisition rate. The intensity was interpolated to generate new image stack and the fitted line of the centroids in the kymograph was calculated. The slope of the fitted line was used to shear the image stack from the flow direction (s) to the optical axis direction (z).

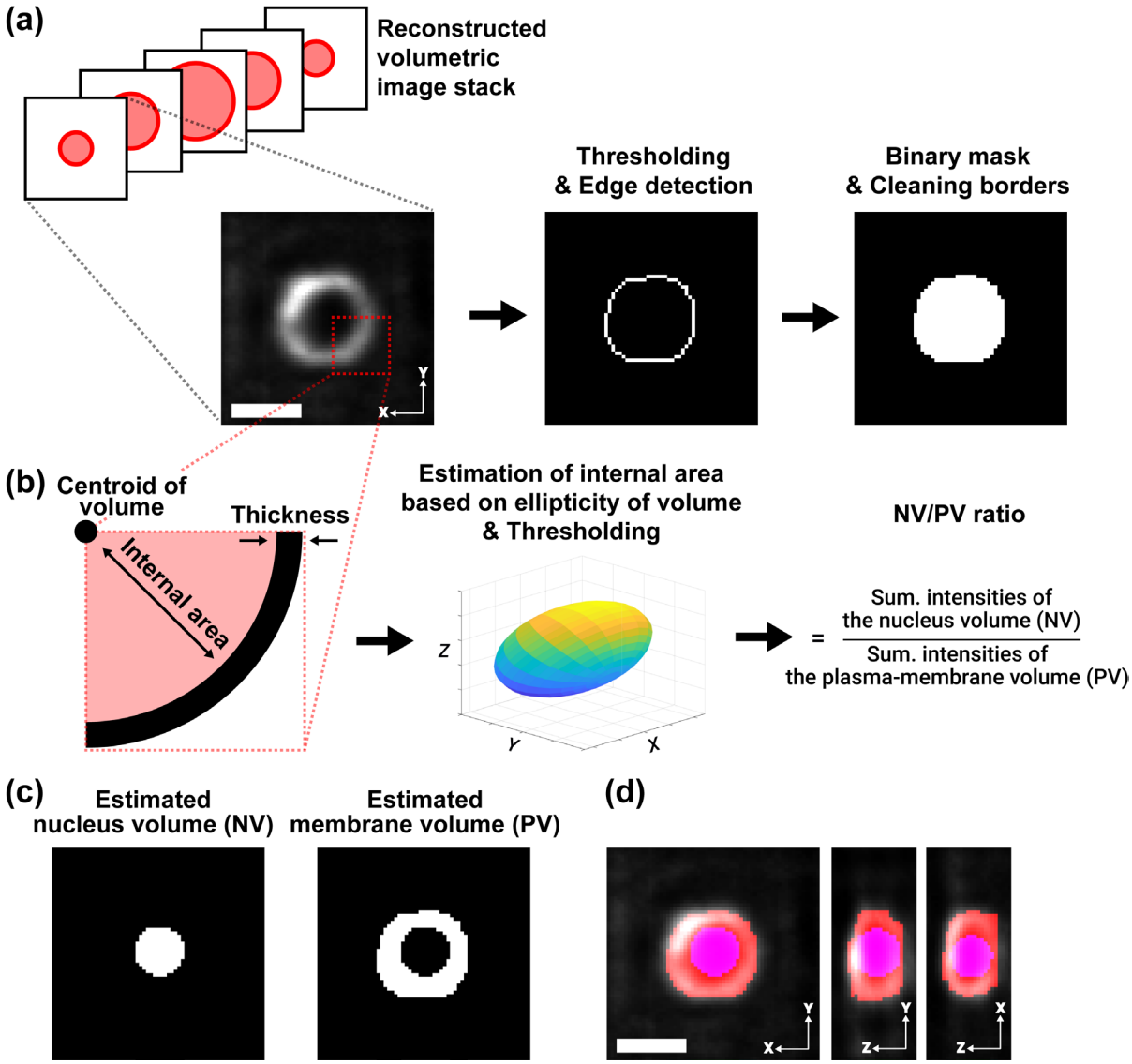

Supplementary Figure S4: The process for volume estimation and NV/PV ratio calculation. (a) The process to estimate the volume from the reconstructed image stack. In each frame, the edge of samples was detected by Sobel operator thresholding and edge detection. Then, the discontinued border lines were removed with dilating linear structuring elements, (a middle). The example shows a reconstructed image of a plasma membrane-stained HeLa cell at the focal plane. The final binary image was generated by filling the internal regions and cleaning borders. (a, right). A binary image stack was used to calculate the estimated volume by multiplying the total number of pixels and a single voxel size. (b) The size of the plasma membrane-stained structure was estimated as 15% of the diameter of the binary image at the focal image, about averaged 7 pixels (3.36 μm). Based on the 3D centroids and the ellipticity by the Regionprops3 function in MATLAB, the nucleus area was estimated. The effective nucleus volume is limited by double thresholds of intensities to refrain from including artifacts. Finally, the NV/PV ratio was calculated by total intensities in the effective nucleus volume (NV) over the estimated plasma membrane-stained volume (PV). (c) The binary images of the estimated nucleus and the plasma membrane at the focal plane of the image stack in (a). (d) The color-coded 3D views of the reconstructed HeLa cell at the focal plane. The red color denotes the estimated volume and the blue color shows the estimated nucleus in x-y (left), y-z (middle), and x-z (right) views. Scale bar: (a, d) 10 μm.

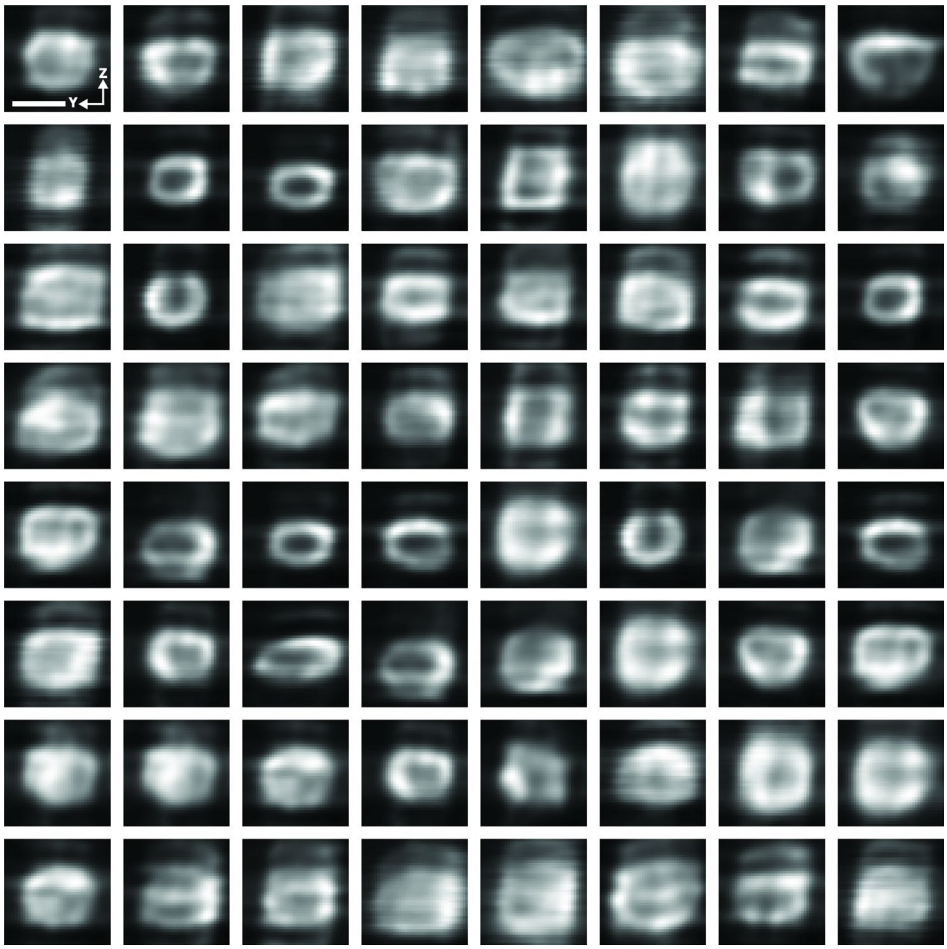

Supplementary Figure S5: The images of plasma membrane stained HeLa cells. The volumetric reconstructed images of plasma membrane-stained HeLa cells in Fig. 3. The representative 64 cells show the projected views of HeLa cells in Y-Z dimension. Scale bar: 10 μm.

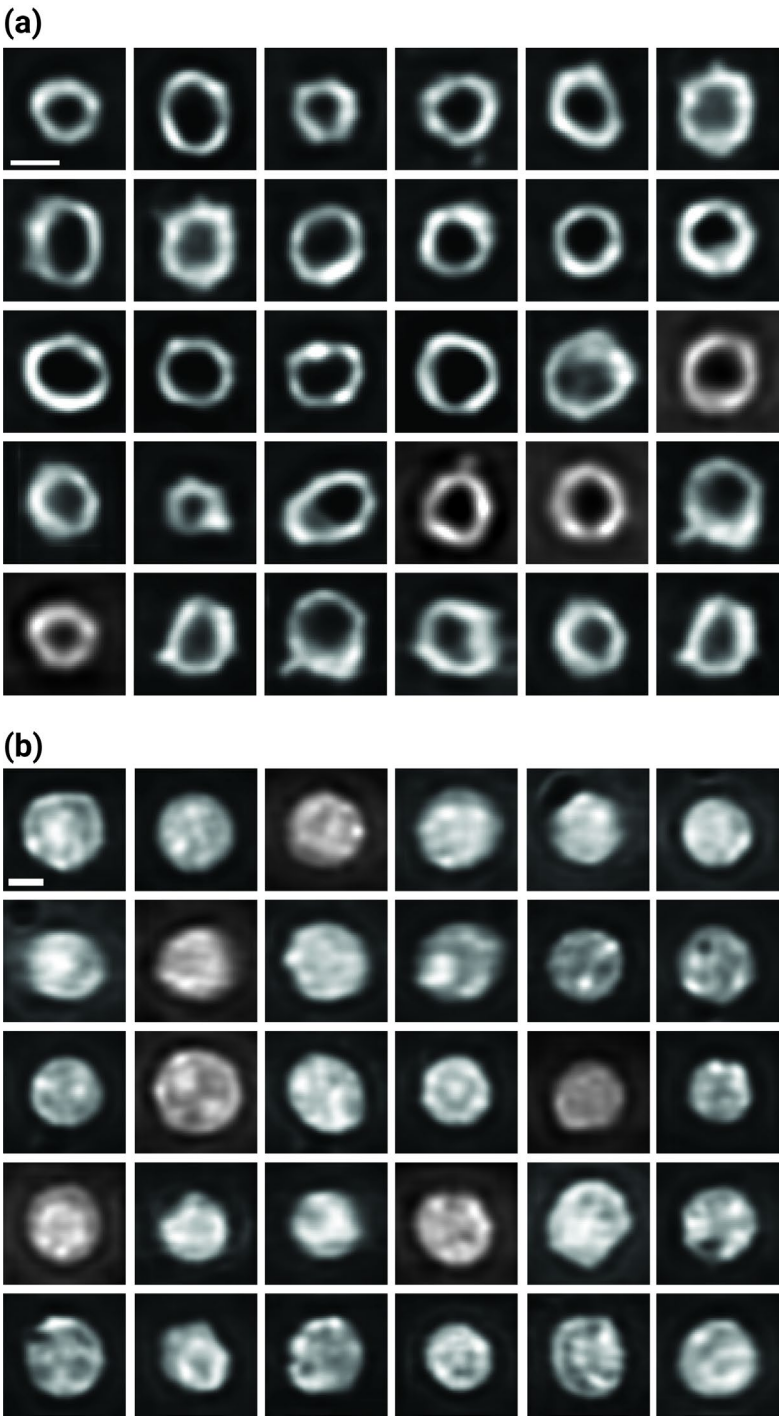

Supplementary Figure S6: Reconstructed images of reconstructed HeLa cells in untreated group (a) and Taxol-treated group (b) in Fig. 5. Cross-sectional images of the representative population show the cytotoxicity assay and PLSOM allows us to label the membrane of both cell groups while only the nuclei of those drug-affected cells that possess compromised plasma membrane. Scale bars: 10 μm (a, b).

Microscope technique	Open-top configuration	Portability of system	Compatibility with commercial microfluidic chips	Throughput	Optical setup	Spatial resolution	Samples
Refractive index-matching tubes [8]	No	No	No	Not provided	SPIM	0.65 µm Lat.	MCF7 cells, Zebrafish embryos and larvae
Novel microchannels [9]	No	No	No	30 samples/min.	SPIM	5.5 µm Axi. @ 532nm exi.	Fixed tissue spheroids
Novel microchannel [10]	No	No	No	1 sample/sec.	SPIM	0.51µm Lat. @ 650nm emi. 2.10 - 4.88 µm Axi. @ 532nm exi.	Human mammary epithelial cells and xenograft-derived primary tumor cells
Imaging capillaries [11]	No	No	No	0.5 µl/min. Volume flow rate	SPIM	0.81 ± 0.07 µm Lat. 1.42 ± 0.15 µm Axi.	Phytoplankton (Gambierdiscus sp. and Procentrum sp.)
Imaging capillaries [12]	No	No	No	2,000 cells/sec.	OPM	0.57 µm Lat. 1.1 - 2.0 µm Axi.	K562 chronic myelogenous leukemia cells
Imaging capillaries [13]	No	No	No	1,200 cells/sec.	SPIM	0.88 µm Lat. 1.34 µm Axi.	K562 cells
Microfabrication of optical elements on a chip [14]	No	No	No	8 cells/sec	SPIM	0.65 µm Lat. 1.8 ± 0.2 µm Axi. @ 480nm exi. @ 520 nm emi	Human Keratinocyte cells, human fibroblast cells, HEK 293 cells, HeLa cells
Engineered microfluidic chips [15]	No	No	No	Not provided	Upright-lattice LSM	2.5 ± 0.2 µm Axi. @ 560nm exi.	CHO cells
Imaging microfluidic chips [16]	No	No	No	30 samples/min.	Droplet-based microfluidic chip	Not provided	Droplets
Imaging microfluidic chips [17]	No	No	Yes	40 cells/sec.	SPIM	3.75 µm Axi. @532nm exi.	HeLa cells
Imaging microfluidic chips [18]	No	No	Yes	2,090 cells/min.	SPIM	7.5 µm Axi. @532nm exi.	Saccharomyces cerevisiae cells
Imaging microfluidic chips [19]	No	No	Yes	800 cells/min.	SPIM	3.14 µm Lat. 3.75 µm Axi.	HeLa cells
PLSOM (Imaging microfluidic chips)	Yes	Yes	Yes	1,000 cells/sec.	Open-top LSM	2.9 µm Lat. 3.4 µm Axi. @ 660nm exi. @ 680nm emi.	HeLa cells, Jurkat cells, human T cells

Table S1: 3D-optofluidic imaging techniques based on fluorescence light-sheet approach. The table provides a summary of representative 3D-fluorescence optofluidic imaging systems and the comparison. LSM: light-sheet microscopy. SPIM: Single-plane illumination microscopy. OPM: Oblique-plane microscopy. PLSOM: Portable light-sheet optofluidic microscopy. min.: minute. sec.: second. exi.: excitation. emi.: emission. Lat.: Lateral resolution. Axi.: Axial resolution. The portability of system was determined in the author's subjective decision based on the overall system size for illumination and detection. The compatibility with commercial microfluidic chips were decided by the author's subjective matter based on the claims in each publication.

Supplementary References

1. M. Kaur and L. Esau, *Biotechniques*, 2015, **59**, 119-126.
2. A. Mielgo, V. A. Torres, K. Clair, S. Barbero and D. G. Stupack, *Oncogene*, 2009, **28**, 3551-3562.
3. P. De, J. H. Carlson, B. Leyland-Jones, C. Williams and N. Dey, *Scientific reports*, 2018, **8**, 1-10.
4. B. Mandracchia, X. Hua, C. Guo, J. Son, T. Urner and S. Jia, *Nature communications*, 2020, **11**, 1-12.
5. J.-Y. Tinevez, N. Perry, J. Schindelin, G. M. Hoopes, G. D. Reynolds, E. Laplantine, S. Y. Bednarek, S. L. Shorte and K. W. Eliceiri, *Methods*, 2017, **115**, 80-90.
6. D. Sage, L. Donati, F. Soulez, D. Fortun, G. Schmit, A. Seitz, R. Guiet, C. Vonesch and M. Unser, *Methods*, 2017, **115**, 28-41.
7. R. Wollman and N. Stuurman, *Journal of cell science*, 2007, **120**, 3715-3722.
8. E. J. Gualda, H. Pereira, T. Vale, M. F. Estrada, C. Brito and N. Moreno, *Biomedical optics express*, 2015, **6**, 4447-4456.
9. P. Paiè, F. Bragheri, A. Bassi and R. Osellame, *Lab on a Chip*, 2016, **16**, 1556-1560.
10. F. Sala, M. Castriotta, P. Paiè, A. Farina, S. D'Annunzio, A. Zippo, R. Osellame, F. Bragheri and A. Bassi, *Biomedical optics express*, 2020, **11**, 4397-4407.
11. J. Wu, J. Li and R. K. Chan, *Optics Express*, 2013, **21**, 14474-14480.
12. M. Ugawa and S. Ota, *Small Science*, 2022, 2100126.
13. M. Ugawa and S. Ota, *Biomedical Optics Express*, 2022, **13**, 3647-3656.
14. E. J. Vargas-Ordaz, S. Gorelick, H. M. York, B. Liu, M. L. Halls, S. Arumugam, A. Neild, A. de Marco and V. J. Cadarso, *Lab on a Chip*, 2021, **21**, 2945-2954.
15. Y.-J. Fan, H.-Y. Hsieh, S.-F. Tsai, C.-H. Wu, C.-M. Lee, Y.-T. Liu, C.-H. Lu, S.-W. Chang and B.-C. Chen, *Lab on a Chip*, 2021, **21**, 344-354.
16. H. Jiang, T. Zhu, H. Zhang, J. Nie, Z. Guan, C.-M. Ho, S. Liu and P. Fei, *Lab on a Chip*, 2017, **17**, 2193-2197.
17. R. Regmi, K. Mohan and P. P. Mondal, *AIP Advances*, 2014, **4**, 097125.
18. R. Regmi, K. Mohan and P. P. Mondal, *Microscopy research and technique*, 2013, **76**, 1101-1107.
19. P. Kumar, P. Joshi, J. Basumatary and P. P. Mondal, *Scientific reports*, 2022, **12**, 1-15.